



Detection of Lung Nodules Triumph Over by Ribs and Clavicles with Multi Scale Approximation Substantial Trained Artificial Neural Network

S Sri Iswarya Lakshmi

*Department of Electronics Communication Engineering
Rajiv Gandhi College of Engineering
Sriperumbudhur, Chennai-602105.*

E Sudha

*Department of Electronics Communication Engineering,
Vels university,
Tambaram, Chennai-600117.*

Abstract- When lung nodules super impose with ribs or clavicles in chest radiographs, it can be tough for radiologists as well as computer-aided diagnostic design to recognize these nodules. In this theory, we evolved an image-processing method for triumph over the contrast of ribs and clavicles in chest radiographs by means of a multi scale substantial trained artificial neural network (s-TANN). An s-TANN is a eminently nonlinear filter that can be trained by use of input chest radiographs and the correlate with “training” images. We manipulated “bone” images acquired by use of a twin-energy deduction method as the training images. For adequate suppression of ribs having numerous spatial frequencies, we evolved a multi scale s-TANN be composed of multi scale integration and Disintegrate methods and three s-TANNs for three different-scale images. Subsequently trained with input chest radiographs and the equivalent twin-energy bone images, the multi scale s-TANN was efficient to afford “bone-image-like” images which were identical to the training bone images. By deducting the bone-image-like images from the equivalent chest radiographs, we were efficient to yield “soft-tissue-image-like” images where ribs and clavicles were substantially suppressed. We depleted a affirmation test database be composed of 118 chest radiographs with pulmonary nodules and an individualistic test database be composed of 136 digitized screen-film chest radiographs with 136 solitary pulmonary nodules collected from 14 medical institutions in this study. When our method was be significant to non-trained lung nodules, ribs and clavicles in the chest radiographs were triumph over substantially, while the perceptibility of nodules and lung vessels was maintained. Thus, our image-processing method for rib suppression by means of a multi scale s-TANN would be probably advantageous for radiologists as well as for CAD design in investigation of lung nodules on chest radiographs.

Keywords- Artificial neural network, chest radiography, computer-aided diagnosis (CAD), twin-energy deduction, lung nodule, rib

I. INTRODUCTION

Chest radiography is the most constantly depleted diagnostic imaging exploration for chest diseases such as lung cancer, tuberculosis, pneumonia, pneumoconioses, and pulmonary emphysema. More than 9 million people globally die annually from chest diseases [1]. Lung cancer causes 945 000 deaths [1], and is the major cause of cancer deaths in the world [1] and in countries [2] such as the United States, the United Kingdom, the Russian Federation, Canada, Poland, and Japan. In the United States alone, lung cancer is look for to cause 160 440 deaths in 2004 [3]. Chest radiographs have been depleted for investigation of lung cancer [4-6] because some affirmation suggests that early investigation of lung cancer may permit a favor efficient prognosis [7-9]. Lung nodules in chest radiographs, however, can be fail to notice by radiologists in from 12%–90% of cases in which nodules are visible in retrospect [10, 11]. Many, 82%–95%, of the missed lung cancers were partially enveloped by overlying bones such as ribs and/or a clavicle [10, 11]. Therefore, a computer-aided diagnostic (CAD) scheme [12, 13] for nodule investigation on chest radiographs has been investigated, because the computer prompts indicating nodules could improve radiologists’ investigation accuracy [14-16]. A major challenge in current CAD design [17-27] for nodule investigation on chest radiographs is the investigation of nodules super imposing with ribs, rib crossings, and clavicles, because a majority of false positives are caused by these structures [18, 28]. This results in lowering the sensitivity as well as the specificity of a CAD scheme. Because nodules super imposing with ribs and clavicles were reported to be tough for radiologists to observe [29, 30], investigation of such nodules is important for CAD design. Therefore, the suppression of ribs and clavicles in chest radiographs would be probably advantageous for improving radiologists’ investigation accuracy as well as

the CAD performance. Our purpose in this study was to develop an image-processing method for triumph over the contrast of ribs in chest radiographs by means of a multi scale massive trained artificial neural network (s-TANN).

II. MATERIALS AND METHODS

A. Substantial trained Artificial Neural Network (s-TANN)

In the field of image processing, supervised nonlinear image-processing methods [31-34] based on an artificial neural network (ANN), called a “neural filter” [32] and a “neural edge enhancer” [33, 34], have been investigated for reduction of the quantum mottle (specific noise observed in medical x-ray images) in angiograms and radiographs [35] and for supervised investigation of left ventricular contours traced by cardiologists in angiography [36], respectively. By extending the neural filter and the neural edge enhancer, s-TANNs [37] have been evolved to accommodate the task of distinguishing a specific opacity from other opacities in medical images. s-TANNs have been significant for reduction of false positives in computerized recognition of lung nodules in low-dose computed tomography (CT) [37, 38] and chest radiography [39], for distinction between benign and malignant lung nodules in CT [40]. In our previous studies [37-40], the s-TANNs aimed at classification of regions-of-interest into abnormal or normal; thus, these studies were in the field of pattern investigation, whereas this theory aims at suppression of ribs in chest radiographs, which would be in the field of image processing. The architecture and the trained method of an s-TANN are shown in Figure 1. The s-TANN can be considered to be a eminently nonlinear filter that can be trained with input images and the equivalent “training” images.

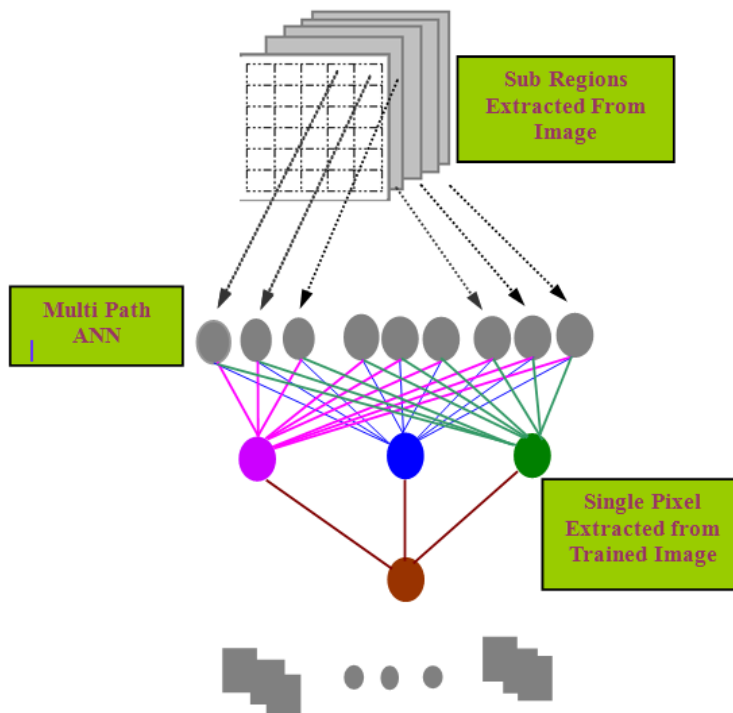


Figure 1: Frame work and training of image consist of a Continuous-output several layer ANN model and a substantial-sub-regions training scheme. The pixel values in the sub-region extracted from a chest radiograph are entered as input to the ANN. Single pixels extracted from images are used as trained values for the corresponding sub-regions

The s-TANN consists of a linear-output multi-layer ANN model [41], which is capable of operating on image data directly. The linear-output multi-layer ANN model employs a linear function instead of a sigmoid function as the activation function of the unit in the output layer because the characteristics of an ANN were improved significantly with a linear function when be significant to the continuous mapping of values in image processing [34, 41]. A conventional ANN hardly outputs values near zero and one because of the characteristics of a sigmoid function, whereas the linear-output multi-layer ANN outputs values linearly. The trained for training values near zero and one converges more slowly than do other values with the conventional ANN theoretically, whereas these values are trained evenly with the linear-output multi-layer ANN model. This affects the convergence characteristics and the output characteristics of ANN models. Therefore, the linear-output

multi-layer ANN would be capable for image processing, where the training values may be continuous values ranging from zero to one, whereas the conventional ANN is capable for a classification task where the training values are assigned to classes (see [34, 41] for theoretical considerations). The pixel values of original chest radiographs are normalized first such that a pixel value of zero is zero and a pixel value of the maximum gray-scale level (1,023) is one. The inputs of the linear-output multilayer ANN are the pixel values in a sub region extracted from a chest radio graph. The output is a continuous value, which corresponds to the center pixel in the sub-region, represented by

$$s(p, q) = XX(\vec{I}_{p,q}) \quad (1)$$

Where

$$I_{p,q} = \{t(p-i, q-j) \mid i, j \in R_c\} \quad (2)$$

is the input vector to the s-TANN $s(p, q)$ is an estimate for a training value, p and q are the coordinates of the image $XX \{\bullet\}$ is the output of the linear-output multilayer ANN $t(p, q)$ and is a normalized pixel value in an input chest radiograph. Note that only one unit is manipulated in the output layer. The input vector can be rewritten as

$$\vec{I}(p, q) = \{I_1, I_2, I_3, \dots, I_m, \dots, I_{NI}\} \quad (3)$$

where m is an input unit number, and NI is the number of input units. Because the activation functions of the units in the input layer are an identity function, the output of the n th unit in the input layer can be represented by I_n . The output of the unit in the hidden layer is represented by

$$O_n^K = fs\{\sum_{m=1}^{N_I} w_{mn}^K \cdot I_m - w_{0n}^K\} \quad (4)$$

where w_{mn}^K is a weight between the m th unit in the input layer and the n th unit in the hidden layer, w_{0n}^K is an offset of the n th unit in the hidden layer, and $fs(x)$ is a sigmoid function

$$fs(x) = \frac{1}{1 + \exp(-x)} \quad (5)$$

The output of the unit in the output layer is represented by

$$f(p, q) = f_L\{\sum_{m=1}^{N_K} w_m^O \cdot O_m^H - w_0^O\} \quad (6)$$

Where w_m^O is a weight between the unit in the hidden layer and the unit in the output layer, w_0^O is an offset of the unit in the output layer, $f_L(x)$ is a linear function

$$f_L(x) = a \cdot x + 0.5 \quad (7)$$

and a is a slope parameter. The entire output image is acquired by scanning of an input chest image with the s-TANN. The s-TANN

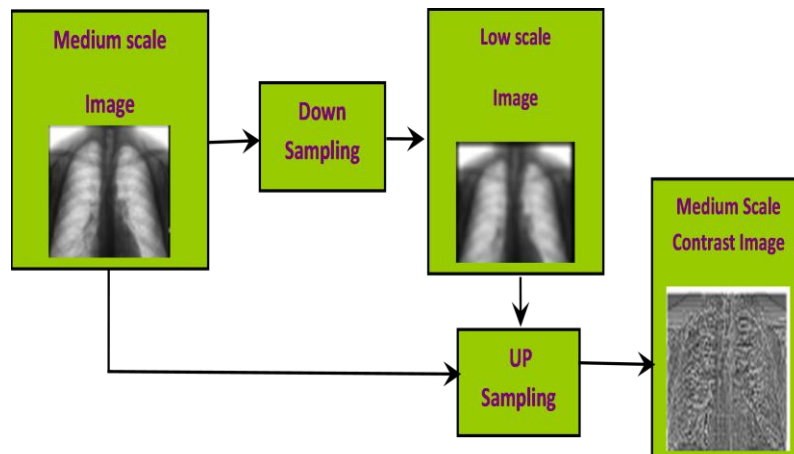


Figure 2: Illustrations of (a) a multi scaling decomposition technique and (b) a multi scaling composition technique. Lower-scale images are produced by repeatedly performing down-sampling and subtracting in a multi scaling decomposition technique.

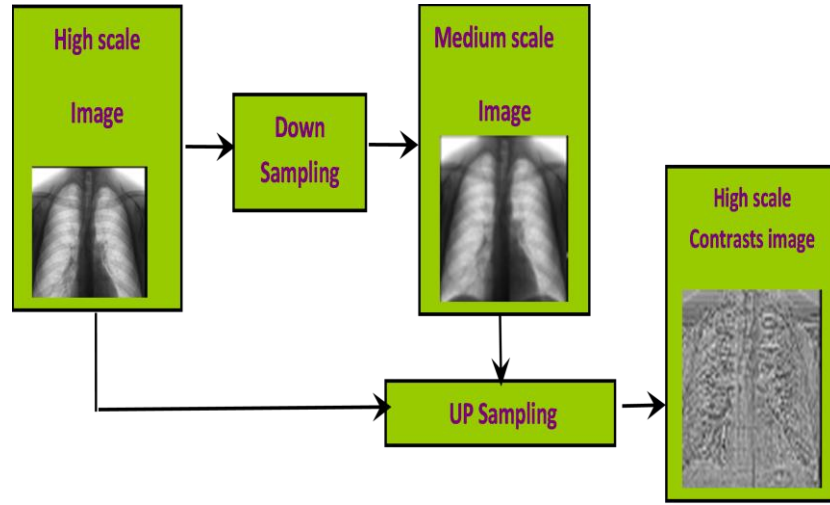


Figure 2: Illustrations of (a) a multi scaling decomposition technique and (b) a multi scaling composition technique. Lower-scale images are produced by repeatedly performing down-sampling and subtracting in a multi scaling decomposition technique.

Involves trained with massive sub-region-pixel pairs, where we call it a massive-sub-regions trained scheme. Input chest radiographs are divided pixel by pixel into a large number of super imposing sub-regions. Single pixels equivalent to the input sub-regions are extracted from the training images as training values. The s-TANN is massively trained by using each of a large number of the input sub-regions together with each of the equivalent training single pixels. The trained set of pairs of a sub-region and a training pixel is represented by

$$\{(\vec{I}(p,q), T_g(p,q) | p, q \in R_{T_g}) = \{(\vec{I}_1, T_{g1}), (\vec{I}_2, T_{g2}), \dots, (\vec{I}_p, T_{gp}), \dots, (\vec{I}_{N_T}, T_{N_T})\} \quad (8)$$

where $T_g(p, q)$ is a training image, R_T is a trained region which corresponds to the collection of the centers of sub-regions (or training pixels), p is a pixel number in R_T , and N_T is the number of pixels in R_T . The error to be minimized by trained is defined by

$$Error = \frac{1}{N_T} \sum_{p,q \in R_T} \{T(p, q) - s(p, q)\}^2 \quad (9)$$

The s-TANN is trained by a linear-output back-propagation (BP) algorithm [34, 41], which was derived for the linear-output multilayer ANN model in the same way as the BP algorithm [42, 43]. The correction of the weight between hidden units and output unit can be represented by

$$\Delta W^o = -\eta \frac{\partial Error}{\partial W^o} = \eta \alpha (T - s) O^H \quad (10)$$

where η is a learning rate. Please refer to [34, 41] for the details and the property of the linear-output BP algorithm. Consequently training, the s-TANN is look for to yield images identical to the training images. We depleted a twin-energy deduction method [44] to obtain the training images for s-TANNs for suppression of ribs in chest radiographs. The twin-energy deduction is a method for separating bones from soft tissues in chest radiographs by use of the energy dependence of the x-ray attenuation by different materials; it can yield two tissue-selective images, i.e., a “bone” image and a “soft-tissue” image. Chest radiographs are depleted as input images to s-TANNs, and the equivalent twin-energy bone images are depleted as the training images. We did not directly use twin-energy soft-tissue images as the training images, because the s-TANNs trained with twin-energy soft tissue images yield results that were slightly inferior to the s-TANNs trained with twin-energy bone images (see details in Section IV).

B. Multi-Scaling Composition/Decomposition

Ribs in chest radiographs include numerous spatial-frequency components. For a single s-TANN, suppression of ribs containing such numerous frequencies is tough because the capability of a single s-TANN is limited, i.e., the capability depends on the size of the sub-region of the s-TANN. Because the trained of the s-TANN takes a substantially long time, it is tough in practice to train the s-TANN with a large sub-region.

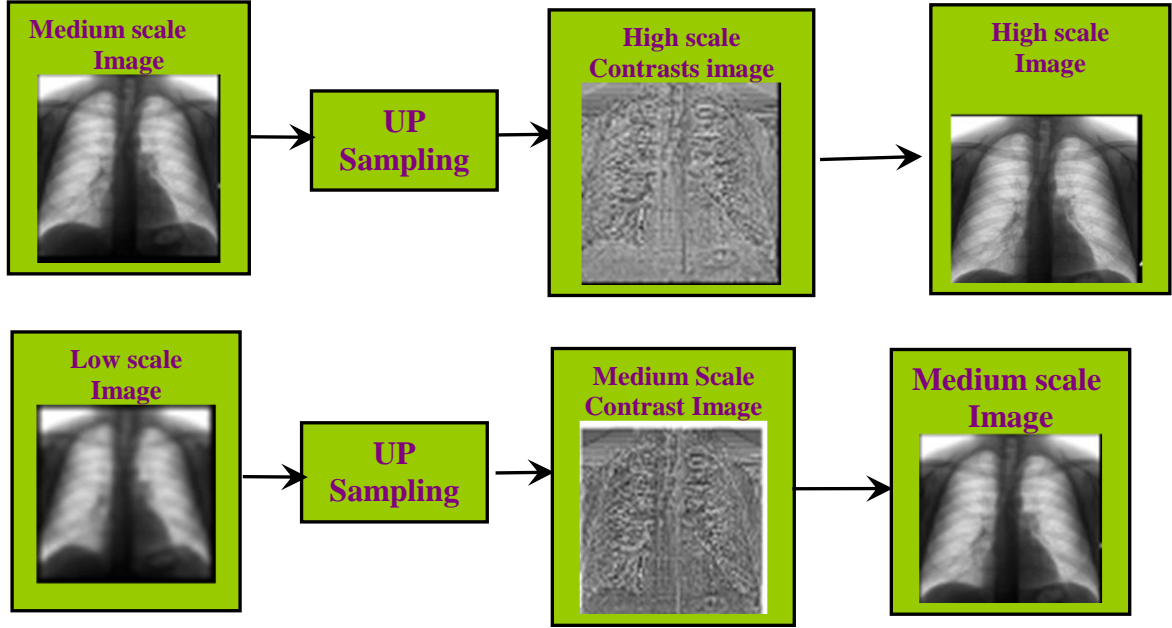


Figure 2: Illustrations of (a) a multi scaling decomposition technique and (b) a multi scaling composition technique. Lower-scale images are produced by repeatedly performing down-sampling and subtracting in a multi scaling decomposition technique. Exactly the same original scale image can be obtained from the multi scale images by performing a multi scale composition technique

In order to overcome this issue, we manipulated multi scale decomposition/ composition methods [45, 46]. The multi scale decomposition, illustrated in Figure 2(a), is a method for decomposing an original high-scale image into different-scale images. First, one obtains a medium-scale image $l_M(p, q)$ from an original high-scale image $l_H(p, q)$ by performing down-sampling with averaging, i.e., four pixels in the original image are replaced by a pixel having the mean value for the four pixel values, represented by

$$l_M(p, q) = \frac{1}{4} \sum_{i,j \in R_{22}} l_H(2p-i, 2q-j) \quad (11)$$

where R_{22} is a 2-by-2-pixel region. The medium-scale image is enlarged by up-sampling with pixel substitution, i.e., a pixel in the medium-scale image is replaced by four pixels with the same pixel value, as follows:

$$l_M^U(p, q) = l_M\left(\frac{p}{2}, \frac{q}{2}\right) \quad (12)$$

Then a high-scale Contrast image is acquired by deduction of the enlarged medium-scale image from the high-scale image, represented by

$$Con_H(p, q) = l_H(p, q) - l_M^U(p, q) \quad (13)$$

These procedures are performed repeatedly, producing further lower-scale images. Thus, multi scale images having numerous frequencies are acquired by use of the multi scale decomposition method. An important property of this method is that exactly the same original-scale image $l_H(p, q)$ can be acquired from the multi scale approximation images $Con_H(p, q)$ and $l_M(p, q)$ by performing the inverse procedures, called a multi scale approximation composition method as shown in Fig. 2(b), as follows:

$$l_H(p, q) = l_M\left(\frac{p}{2}, \frac{q}{2}\right) + Con_H(p, q) \quad (14)$$

Therefore we can process multi scale approximation images independently instead of processing original high-scale images directly; i.e., with these methods, the processed original high-scale image can be acquired by composing of the processed multi scale approximation images. An s-TANN only needs to support a limited spatial frequency range in each scale image instead of the entire spatial frequencies in the original image.

C. Multi scale Approximation s-TANN for triumph over Ribs

Fig.3 illustrates the architecture and trained of a multi scale approximation s-TANN involving multi scale approximation decomposition/composition methods and s-TANNs for different-scale images. First, input chest radiographs and the equivalent training bone images are decomposed into sets of different-scale images, and then these sets of images are depleted for trained three s-TANNs in the multi scale approximation s-TANN, as illustrated in Figure 3(a).

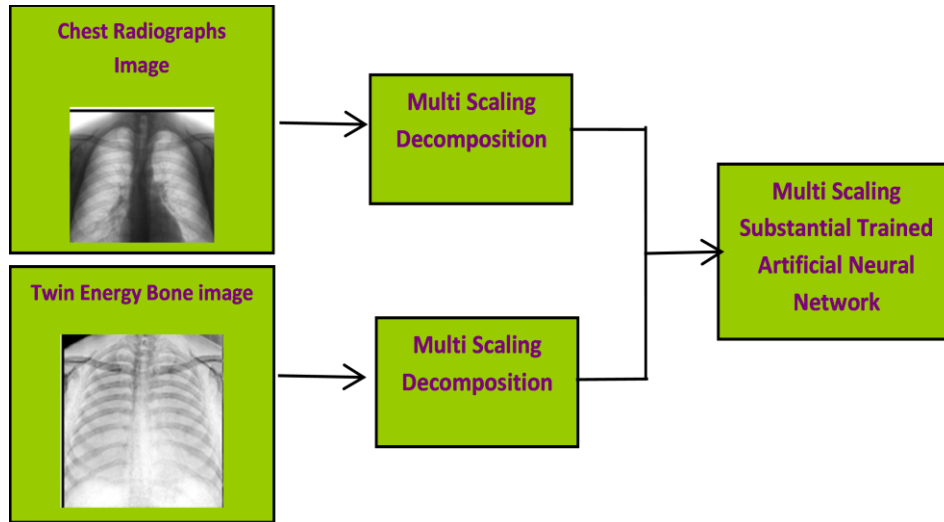


Figure 3: Diagrams of (a) a training phase In the training phase, an input chest radiograph and a training bone image are decomposed in to multi scale images by use of a multi scale decomposition technique. Each of the multi scale images is used for each of the corresponding scale substantial Artificial Neural Network in the multi scale s-TANN

Each s-TANN is an expert for a certain scale, i.e., a low-scale s-TANN is in charge of low-frequency components of ribs, a medium-scale s-TANN is for medium-frequency components and a high-scale s-TANN for high-frequency components. Each scale s-TANN is trained independently with the equivalent scale images. subsequently training, the s-TANNs yield different-scale images, and then these images are composed to afford a complete high-scale image by use of the multi scale approximation composition method, as illustrated in Figure 3(b). The complete high-scale image is look for to be identical to the training bone image; therefore, the multi scale approximation s-TANN would afford a “bone-image-like” image in which ribs are separated from soft tissues.

The multiple s-TANN scheme in our previous studies [37, 40] was evolved for classification of candidates into multiple categories; therefore, the output of the multiple s-TANN scheme is a class, i.e., abnormal or normal, whereas the output of the multi scale approximation s-TANN is a pixel value. In the multiple-s-TANN scheme, s-TANNs were combined with scoring, thresholding, and the logical AND operation, whereas the multi scale approximation s-TANN does not use any of these. In the multi scale approximation s-TANN, the input to each of s-TANNs is certain frequency components acquired from the original images by use of the multi scale approximation decomposition, whereas the input of the multiple s-TANN scheme is pixel values of the original images. In this theory, we focused on the suppression of ribs and clavicles in lung regions, because most nodules super imposing with these structures are in the lung regions. For processing only in the lungs, lung regions are segmented by thresholding. A threshold value is determined by use of a method [47] based on linear discriminant analysis (LDA), which is a common method in the fields of computer vision and pattern investigation. It is look for that a reason capable threshold value can be determined by use of LDA, because threshold determination can be considered as a two-class classification problem in the domain of the histogram of gray levels, and the linear separation with LDA would work well in this one dimensional space. This method automatically selects the lowest point between two classes in the histogram of gray levels in a chest radiograph (i.e., this is formulated as LDA).The method involves minimizing the ratio of between-class variance to the total variance. Subsequently the segmentation, a Gaussian filter is be significant for smoothing the edges of the segmented lung regions to create an image for masking the outside of the lung regions. The masking image is normalized to have values from 0 to 1. For suppression of ribs in an original chest radiograph, the bone-image-like image $f_b(p, q)$ yield by the multi scale s-TANN is subtracted from the original chest.

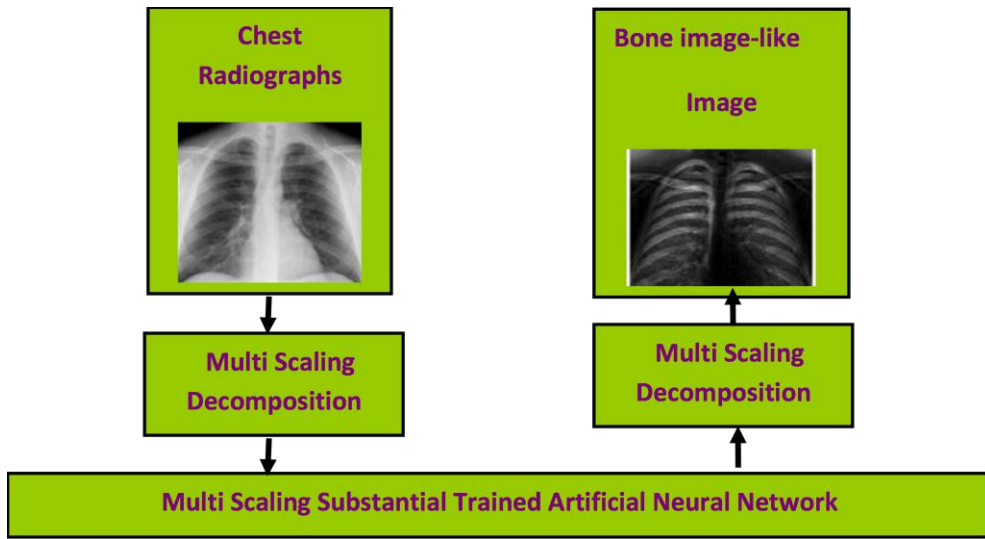


Figure 4: (b) An execution phase of a multi scale network consisting of networks for different-scale images. In the execution phase, the output multi scale images of the trained multi scale network are composed to provide a “bone-image-like” image by use of a multi scale composition technique.

radiograph $l(p, q)$ with the masking image $z(p, q)$ as follows:

$$f_{uv}(p, q) = l(p, q) - w_C * f_b(p, q) * m(p, q) \quad (15)$$

Where w_C is a weighting parameter for determining the contrast of ribs. By changing the weighting parameter w_C , one can obtain processed chest radiographs with different contrast of ribs. Thus, the multi scale approximation s-TANN would be capable to yield a “soft-tissue-image-like” image where ribs are suppressed; therefore, this image processing may be considered as a “rib suppression” method.

D. Database

The database depleted in our study consisted of 133 posterior-anterior chest radiographs acquired with a computed radiography system with a twin-energy deduction unit (FCR 9501 ES; Fujifilm Medical Systems, Stamford, CT) at The University of Chicago Hospitals. The twin-energy deduction unit manipulated a single-shot twin-energy deduction method where image acquisition is performed with a single exposure that is recognized by two receptor plates separated by a filter for obtaining images at two different energy levels [44, 48, 49]. The chest radiographs included 115 abnormal cases with pulmonary nodules and a “normal” case (i.e., a nodule-free case). The matrix size of the chest images was 1,760 1,760 pixels (pixel size, 0.2 mm; gray scale, 10 bits). The absence and presence of nodules in the chest radiographs were confirmed by use of CT explorations. Most nodules superimpose with ribs and/or clavicles in chest radiographs. In order to train a multi scale approximation s-TANN, we depleted a trained set be composed of four chest radiographs and the equivalent twin-energy soft-tissue and bone images.

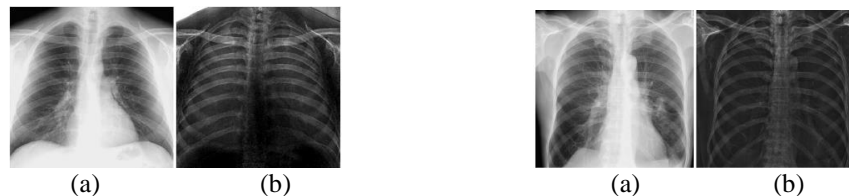


Figure 5: Illustrations of (a) input images and (b) the corresponding training bone images used for training a multi scaling network (upper images: a normal case; lower images: a nodule case).

Three of the four chest radiographs were from nodule cases, and the other was the normal case. The registration error between the input images and the training images would be minimum because of the use of the single-shot twin-energy deduction method.



Figure 6: Illustrations of (a) input images and (b) the corresponding training bone images used for training a multi scaling S-ANN (upper images: a normal case; lower images: a nodule case)

We depleted a test set be composed of 120 nodule cases for testing our method. For computational efficiency, the size of the chest radiographs was reduced by a factor of four, i.e., 440 440 pixels. We depleted another test set be composed of 136 digitized screen-film chest radiographs with 131 solitary pulmonary nodules, which was the Digital Image Database evolved by the Japanese Society of Radiological Technology (JSRT) [50], a publicly capable database. The chest radiographs were collected from 14 medical institutions. The absence and presence of nodules in the chest radiographs were confirmed by CT. The locations of all nodules were confirmed by three chest radiologists. The chest radiographs were digitized with a 0.175-mm pixel size, a matrix size of 2,048 2,048, and a 12-bit gray-scale level. The sizes of nodules ranged from 8.9 to 29.1 mm, and the average size was 17.4 mm. The database contained 64 malignant and 27 benign nodules, which were confirmed by histologic or cytologic explorations or follow-up imaging. For computational efficiency, the size of the chest radiographs was reduced by a factor of four to 512 512 pixels with a 10-bit gray-scale level by use of averaging.

III. RESULTS

A. Training

We depleted four chest radiographs and the equivalent dual energy bone images in a trained set for trained a multi scale approximation s-TANN. One of the important properties of an s-TANN is that it can be trained with a very small number of cases, because an s-TANN is trained with a large number of sub-regions extracted from input images, i.e., an s-TANN can be trained not on a case base, but on a sub-region base [51]. We depleted one typical normal case and three cases with nodules as trained cases. Fig. 4 shows the normal case and an example of a nodule case. For trained of the features in lung regions, 5,000 pairs of trained samples were extracted randomly from manually traced lung regions in each of the multi scale approximation images. Trained samples for nodules were extracted from the manually traced nodule regions which were large enough to cover the nodules.

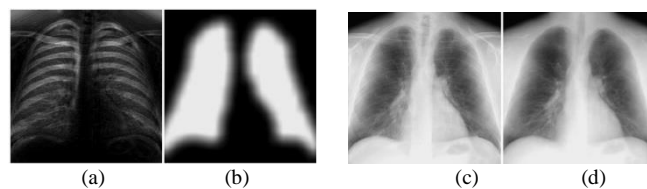


Figure 5: Illustrations of (a) the output image, i.e., a bone-image-like image, of the trained multi scaling network for the upper image in Fig. 4 (a), (b) a masking image for lung regions, (c) a soft-tissue-image-like image obtained by use of our technique, and (d) the corresponding twin-energy soft-tissue image

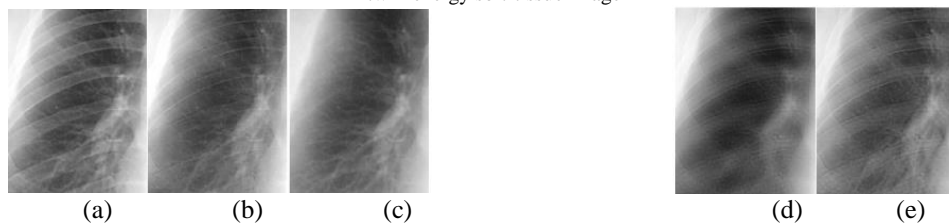


Figure 6: Comparisons among (a) an original image extracted from the upper image in Fig. 4 (a), (b) a soft-tissue-image-like image obtained by use of our technique, (c) a twin-energy soft-tissue image, (d) the output image of the optimized linear filter, and (e) the output image of a single ANN without multi scaling decomposition/composition techniques.

We combined these trained samples and depleted them for trained a multi scale approximation s-TANN. We determined the size of the sub-regions of s-TANNs to be nine by nine pixels, so that the sub-region was sufficient to cover the width of a rib in the low scale image. We depleted three-layered s-TANNs where the numbers of input, hidden, and output units were 81, 20, and 1, respectively. The learning rate was 0.001. With the parameters above, trained of three s-TANNs was performed 1 000 000times, and the trained converged with mean absolute errors of 0.081, 0.086, and 0.017. Fig. 5(a) shows the composed output image, i.e., a

bone-image-like image, of the trained multi scale approximation s-TANN. Ribs are extracted effectively in the bone-image-like image, and this image is identical to the twin-energy bone image shown in Figure 4(b) (upper image). Ribs in the bone-image-like image are relatively noisy compared to the twin-energy bone image. Delicate parts of small vessels remain in the bone-image-like image, which causes the noisy opacity. It will be noted that bones outside the lung regions, such as parts of clavicles and the spinal column, were not enhanced in the bone-image-like image, because the trained was limited to the lung regions. Fig.5(c) shows a soft-tissue-image-like image acquired by use of a weighting parameter of 1.0 and the masking image shown in Figure 5(b). The contrast of ribs is substantially triumph over in the soft-tissue-image-like image, whereas the perceptibility of soft tissues such as lung vessels is maintained. The soft-tissue-image-like image is very identical to the equivalent twin-energy soft-tissue image shown in Figure 5(d). We compared the trained multi scale approximation s-TANN with the linear filter optimized under the least-mean-square error criterion [52] with the same trained images as depleted for the s-TANN. The linear filter consisted of nine-by-nine inputs I_n with 81 weights w_n , represented by

$$V(p, q) = \sum_{n=1}^{81} I_n * w_n \quad (16)$$

where ,

$$\{I_1, I_2, \dots, I_n, \dots, I_{81}\} = \{g(x-i, y-j) \mid i, j \in R_V\}$$

And R_V is a nine-by-nine input region. Fig. 6 shows comparisons between the trained multi scale approximation s-TANN and the optimized linear filter. Ribs are triumph over substantially in the output image of the trained multi scale approximation s-TANN, while maintaining the perceptibility of vessels. The edges of ribs in the output image of the optimized linear filter appear to be doubled and blurred. Moreover, vessels almost disappear. It should be noted that the output images of the optimized linear filter for other chest images had identical perceptibility of ribs and vessels. This result indicated that the capability of the linear filter was not sufficient for separating ribs in chest radiographs. Moreover, we investigated the effect of multi scale approximation decomposition/ composition methods on the performance of an s-TANN. We trained a single s-TANN with the same trained images without the use of multi scale approximation decomposition/composition methods. The parameters for the single s-TANN were the same as those for the multi scale approximation s-TANN. Fig. 6(e) shows the output image of the trained single s-TANN. Parts of ribs are triumph over in the output image, whereas some vessels disappear. This result indicates that the use of multi scale approximation methods in s-TANNs improved the performance in the suppression of ribs and the maintenance of soft-tissue opacities.

B. Analysis and Comparison

We are significant the trained multi scale approximation s-TANN to a affirmation test set that included 118 nodule cases. The performance was evaluated quantitatively by use of a normalized mean absolute error between $f_b(p, q)$ bone-image-like images and the equivalent twin-energy bone images $b_n(p, q)$, represented by

$$Error_N = \frac{\sum_{p, q \in R_V} |b_n(p, q) - f_b(p, q)|}{N_V (b_{n_{\max}} - b_{n_{\min}})} \quad (17)$$

where R_V indicates lung regions, N_V is the number of pixels in R_V , b_{\max} and b_{\min} are the maximum value and the minimum value in R_V in the twin-energy bone image, respectively. We depleted bone-image-like images and twin-energy bone images in this evaluation, because the direct comparison with the output images of the multi scale approximation s-TANN would be more accurate compared to the use of soft-tissue-image-like images, e.g., soft-tissue-image-like images can differ when a weighting parameter is changed. The result for the 118 chest radiographs was an average EN of 0.082 with a standard deviation of 0.014. Figs. 7–9 show the soft-tissue-image-like images and the equivalent twin-energy soft-tissue images. Fig. 7 shows a case with the best value among the 118 nodule cases, EN which is 0.061. The contrast of ribs is substantially triumph over in the soft-tissue-image-like image, while the perceptibility of soft tissues such as lung vessels is mostly maintained. The soft-tissue-image-like image is very identical to the twin-energy soft-tissue image. Fig. 8 illustrates cases with about a middle ranking in EN values, which are 0.078 and 0.080. In original chest radiographs shown in Figure 8(a), a nodule super imposes completely with an anterior rib and partially with posterior ribs in the upper case, and a nodule super imposes with a posterior rib in the lower case. In the soft-tissue-image-like images, the opacities of the super imposing ribs are compensated for substantially, and the true shapes of the nodules are evident. Thus, the distinction between nodules super imposing with ribs and other anatomic structures is improved in the soft-tissue-image-like images. Fig. 9 shows a case with the worst value, EN which is 0.139.

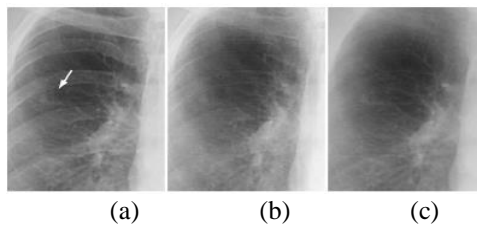


Figure 7: Result for a non training chest radiograph with the best average normalized error among 118 nodule cases in a validation test. Illustrations of (a) an original chest radiograph (nodule is indicated by an arrow), (b) a soft-tissue-image-like image obtained by use of our technique, and (c) the corresponding twin energy soft-tissue image.

The ribs are not triumph over very much in the soft-tissue-image-like image in this case. Our method did not work well for this case, probably because the contrast of ribs in the original chest radiograph of this case was higher than that in other chest radiographs due to the patient's spare frame, i.e., the acquisition condition would be different, and the clavicles at an acute angle indicated that this case would be taken for some special purpose. By inclusion of cases with high rib contrast in trained cases, the performance of a multi scale approximation s-TANN for such cases would be improved.

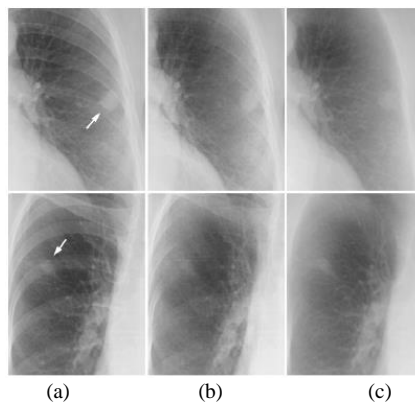


Figure 8: Results for non raining chest radiographs with about a middle ranking in average normalized errors among 118 nodule cases in a validation test. Illustrations of (a) original chest radiographs (nodule is indicated by an arrow), (b) soft-tissue-image-like images obtained by use of our technique, and (c) the corresponding twin-energy soft-tissue images

To investigate the robustness of our method, we performed another experiment with an individualistic test database including 136 nodule cases acquired from 14 medical institutions [50]. These cases were digitized from films and were acquired at numerous settings with numerous systems. We be significant the trained multi scale approximation s-TANN to the individualistic test database. The performance regarding the nodule perceptibility was evaluated quantitatively by use of a nodule contrast defined by the Contrast between an average gray level in a nodule region g_N and a background gray level, represented by $C = g_N - g_B$. The nodule region was determined by two expert chest radiologists by the following method: One of the two radiologists determined an initial nodule region, and then the final nodule region was determined by modifying of the initial nodule region by a consensus between the two radiologists. The background gray level was determined as a pixel value at the lower 10% in the histogram of pixel values in a background region in order to avoid the effect of noise. The background region was determined as a belt-like region with a 10 mm width which was acquired by deducting the nodule region from the dilated nodule region. To evaluate how much the contrast of a nodule is maintained, We defined a nodule contrast ratio represented by, $CR = CM/CO$ where CM is the nodule contrast in

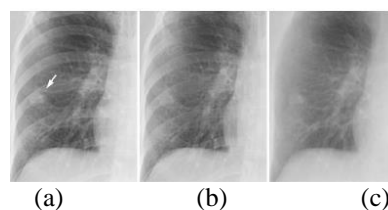


Figure 9: Result for a non training chest radiograph with the worst average normalized error among 118 nodule cases in a validation test. Illustrations of (a) an original chest radiograph (nodule is indicated by an arrow), (b) a soft-tissue-image-like image obtained by use of our technique, and (c) the corresponding twin-energy soft-tissue image

s-TANN soft-tissue-image-like image, CO and is the nodule contrast in an original chest image. An average nodule contrast ratio over 136 nodules was 0.906 with a standard deviation of 0.155. Figs. 10–12 show soft tissue-image like images and the equivalent twin-energy soft-tissue images.

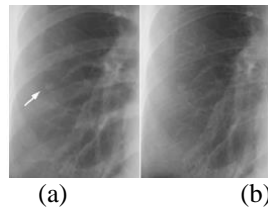


Figure 10: Result for a non training chest radiograph with the best nodule contrast ratio among 136 nodule cases in an independent test. Illustrations of (a) an original chest radiograph (nodule is indicated by an arrow) and (b) a soft-tissue-image-like image obtained by use of our technique

Fig. 10 shows a case with the best CR value among the 136 nodule cases, which is 1.139.

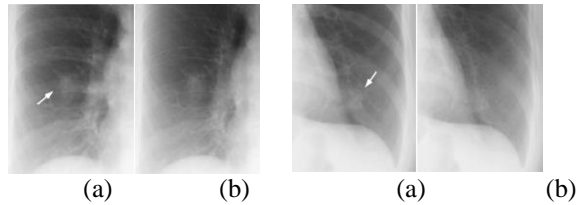


Figure 11: Results for non training chest radiographs with about a middle ranking in the nodule contrast ratio among 136 nodule cases in an independent test. Illustrations of (a) original chest radiographs (nodule is indicated by an arrow) and (b) soft-tissue-image-like images obtained by use of our technique.

The contrast of ribs is triumph over substantially in the soft-tissue-image-like image, whereas the contrast of a nodule is maintained. Thus, the perceptibility of the nodule is improved by suppression of the ribs around the nodule. Fig.11 illustrates two cases with about a middle ranking in values, which are both 0.897. The contrast of nodules is mostly maintained in the soft-tissue-image-like images, whereas super imposing ribs are triumph over substantially. Fig.12 shows a case with the worst value, which is 0.620. The ribs are triumph over in the soft-tissue-image-like image, whereas most parts of the nodule disappear. Our method did not work well for this case, probably because this particular nodule had characteristics identical to those of ribs in terms of

- the shape of the nodule,
- the contrast, the orientation,
- the texture, the margin

IV. DISCUSSION

A twin-energy deduction method [53, 54] has been depleted to address the issue of obscuring bones. twin-energy chest radiographs can be acquired by either a rapid sequence of two exposures, each at a different energy level [e.g., one at 60–80 kV and the other at 110–150 kV] [55–58], or a single exposure that is recognized by two receptor plates separated by a filter for obtaining images at two different energy levels [44, 48, 49]. Twin-energy soft-tissue images can improve the recognized of focal soft-tissue opacities, such as lung nodules, that may be partially enveloped by overlying ribs or clavicles [29, 30, 59]. In spite of the advantages, a very limited number of hospitals use radiography systems with twin-energy deduction, because specialized equipment for obtaining twin-energy X-ray exposures is required. Also, the radiation dose can be greater than that for standard chest radiography in some cases. In addition, the deduction of two-energy images causes an increased noise level in the images.

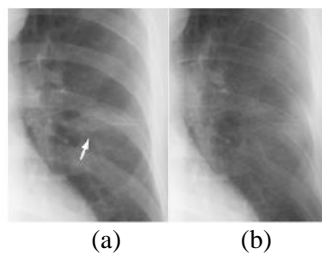


Figure 12: Result for a non training chest radiograph with the worst nodule contrast ratio among 136 nodule cases in an independent test. Illustrations of (a) an original chest radiograph (nodule is indicated by an arrow) and (b) a soft-tissue-image-like image obtained by use of our technique.

For improvement in the signal-to-noise ratio, in previous studies, the average skin entrance radiation dose with the two-exposure twin-energy method was 119 to 130 mR [60, 61], and that with the single-exposure twin-energy method was 60–100 mR [44], both of which are greater than the 15–20 mR depleted in standard chest radiography. In a recent study, a 2.4 times higher radiation dose was depleted for twin-energy radiography compared with conventional radiography in order to obtain the same noise level [62]. The major advantages of our method compared to a twin-energy deduction method are that our method requires no additional radiation dose to patients, but uses only chest radiographs acquired with a standard radiography system for producing soft-tissue-image-like images; and no specialized equipment for generating twin-energy x-ray exposures, but only software, is required. A current limitation of conventional chest radiography would be a relatively low sensitivity for recognized of early cancer. Likewise twin-energy soft-tissue images, s-TANN soft-tissue-image-like images have a potential to improve the sensitivity in recognizing early cancer that is partially enveloped by overlying ribs, and a potential to improve the specificity by differentiating nodules from other abnormalities or normal anatomic structures better because of the suppression of obscuring ribs.

We acquired bone-image-like images and soft-tissue-image like images by use of our method that was trained with dual energy bone images. We investigated the effect of the direct use of twin-energy soft-tissue images as the training images for a multi scale approximation s-TANN. In the soft-tissue-image-like images acquired by use of the multi scale approximation s-TANN trained with twin-energy soft-tissue images, the contrast of lung vessels was relatively low, and some details of the soft tissue disappeared. The use of twin-energy soft-tissue images as the training images was not adequate compared to the use of twin-energy bone images probably because the pattern variations of soft tissues are greater than those of ribs. One advantage of trained with twin-energy bone images is that a different contrast of ribs can be acquired by changes in a weighting parameter in the deduction process depleted for our method. Our method, likewise the twin-energy deduction method, can be sensitive to noise due to deduction. However, our method uses standard-dose chest radiographs as input, whereas the twin-energy deduction method uses two half-dose chest images and subtracts them. Therefore, our method would be advantageous, in theory, in terms of the quantum noise level. One way of improving the quantum noise property of both methods would be to acquire chest images with a higher radiation dose. We depleted a very small number of cases for trained the multi scale approximation s-TANN, and the multi scale approximation s-TANN yield capable results for non trained cases. However, a multi scale approximation s-TANN would be more robust against variations among cases if a larger number of cases were depleted for training. A major challenge in current CAD design is the recognition of nodules super imposing with ribs and clavicles, because most false positives are caused by these structures [18, 28, 39]. Consequently, some researchers have investigated CAD design for recognition of nodules on twin-energy radiographs [63, 64]. The distinction between nodules and other anatomic structures such as ribs and clavicles is improved in soft-tissue-image-like images with our method; therefore these images have the potential to improve the performance of nodule-recognition CAD design. Because the use of a multi scale approximation s-TANN requires only software this method can be utilized on an existing viewing workstation. The processing time for creating a soft-tissue-image-like image and a bone-image-like image from a chest radiograph is very short ,i.e., 1.63 s on a PC-based workstation (CPU: Intel Pentium IV, 3.2 GHz) thus, the software can be be significant prior to interpretation in every case without incurring any delay. Because the fine structures of soft tissues such as small vessels are mostly maintained in soft-tissue-image-like images, the images could probably be depleted for quantitative assessment of interstitial lung diseases which are characterized by fine patterns.

If our method is be significant to anatomic regions other than the lungs in x-ray images, trained with twin-energy images of these anatomic regions would be required for accurate bone suppression. The multi scale approximation decomposition/composition methods with two down/up-sampling steps permitted s-TANNs to support a 28.8-by-28.8 mm square region. The height of a posterior rib would range roughly from 10 to 20 mm. We reduced the size of the original chest images by a factor of four before our method was be significant. Because of this reduction, the pixel size was changed from 0.2 to 0.8 mm. In order to process original-scale chest images with a pixel size of 0.2 mm, we need two more steps of down/up-sampling to support the height of a rib sufficiently. By use of four steps of down/up-sampling, s-TANNs can support a 28.8-by-28.8 region in the original-scale chest images. The number of s-TANNs needs to be increased to be five. We expect that the s-TANNs with original-scale chest images would yield better images containing the details of soft tissue because of the use of higher-scale images. We manipulated a three-layer structure for the structure of the s-TANNs, because it has been proved theoretically that any continuous mapping can be realized approximately by three layer ANNs [65, 66]. The number of hidden units was determined by use of a method for determining the structure of ANNs [67]. The method is a sensitivity-based pruning method, i.e., the sensitivity to the trained error was calculated when a certain unit was removed experimentally, and the unit with the smallest trained error was removed. Removing the redundant hidden units and retrained for recovering the potential loss due to the removal were performed repeatedly, resulting in a reduced structure where redundant units were removed. As a result, the number of hidden units was determined to be 20. Thus, the numbers of units in the input, hidden, and output layers were 81, 20, and 1, respectively. The trained of an s-TANN seeks to minimize errors between output images and training bone images. The quality of the training bone images would affect the output image of the

trained s-TANN, and thus, the final soft-tissue-image-like images. A way to improve the quality of the training bone images would be to acquire training bone images with a higher radiation dose to reduce quantum noise. The relatively high-dose bone images should be depleted only for training. Once training is completed, the trained s-TANN can be significant to standard dose chest radiographs. An s-TANN is an eminently nonlinear complex model. A complex model usually tends to have poor generalization ability. If a model is trained with only a small number of samples, the generalization ability will be lower, i.e., the model may fit only the trained samples; this is known as “over-training”(or “over-fitting”) [68]. This issue often occurs when the number of freedoms (parameters) in a model is greater than the number of trained samples. A study showed that a standard ANN with 100 parameters required 400–800 trained samples to achieve an adequate performance for non-trained cases [69]. The number of trained samples was 4–8 times greater than the number of parameters in the ANN. On the other hand, the results with the individualistic database in this theory showed that s-TANNs have a high generalization ability, which is consistent with what we experienced in other applications [37-40]. In our previous study, we found that a key to the high generalization ability of s-TANNs is the massive training with a large number of sub regions extracted from images [70]. In this study, the number of trained samples for each s-TANN, which was 7100 (5000 sub regions from a normal case and 2100 sub regions from nodule cases), was 4.3 times greater than the number of parameters of the s-TANN, which was 1,661. This is within the above range (4–8 times) for obtaining an adequate performance for non-trained cases. Thus, the number of trained samples might have reached a necessary number for determining the parameters in the s-TANNs adequately.

V. CONCLUSION

We evolved an image-processing method for suppression of ribs in chest radiographs by means of a multi scale approximation s-TANN. With our method, rib components in chest radiographs are removed substantially, while soft-tissues such as lung nodules and lung vessels are maintained. Therefore, our method would be probably advantageous for radiologists as well as for CAD design in the recognition of lung nodules in chest radiographs.

REFERENCES

- [1] C. J. Murray and A. D. Lopez, “Mortality by cause for eight regions of the world: global burden of disease study,” *Lancet*, 349(9061), pp. 1269–1276, 1997.
- [2] G. E. Goodman, “Lung cancer. 1: prevention of lung cancer,” *Thorax*, 57(11), pp. 994–999, 2002.
- [3] A. Jemal, R. C. Tiwari, T. Murray, A. Ghafoor, A. Samuels, E. Ward, E.J. Feuer, and M. J. Thun, “Cancer statistics, 2004,” *CA. Cancer J. Clin.*, 54(1), pp. 8–29, 2004.
- [4] J. K. Frost, W. C. Ball Jr., M. L. Levin, M. S. Tockman, R. R. Baker, D. Carter, J. C. Eggleston, Y. S. Erozan, P. K. Gupta, and N. F. Khouri et al., “Early lung cancer detection: results of the initial (prevalence) radiologic and cytologic screening in the Johns Hopkins study,” *Am. Rev. Respir. Dis.*, 130(4), pp. 549–554, 1984.
- [5] R. S. Fontana, D. R. Sanderson, W. F. Taylor, L. B. Woolner, W. E. Miller, J. R. Muhm, and M. A. Uhlenhopp, “Early lung cancer detection: results of the initial (prevalence) radiologic and cytologic screening in the Mayo Clinic study,” *Am. Rev. Respir. Dis.*, 130(4), pp. 561–565, 1984.
- [6] C. I. Henschke, O. S. Miettinen, D. F. Yankelevitz, D. M. Libby, and J. P. Smith, “Radiographic screening for cancer. Proposed paradigm for requisite research,” *Clin. Imag.*, 18(1), pp. 16–20, 1994.
- [7] R. T. Heelan, B. J. Flehinger, M. R. Melamed, M. B. Zaman, W. B. Perchick, J. F. Caravelli, and N. Martini, “Non-small-cell lung cancer: results of the New York screening program,” *Radiology*, 151(2), pp. 289–293, 1984.
- [8] T. Sobue, T. Suzuki, M. Matsuda, T. Kuroishi, S. Ikeda, and T. Naruke, “Survival for clinical stage I lung cancer not surgically treated. Comparison between screen-detected and symptom-detected cases. The Japanese Lung Cancer Screening Research Group,” *Cancer*, 69(3), pp. 685–692, 1992.
- [9] B. J. Flehinger, M. Kimmel, and M. R. Melamed, “The effect of surgical treatment on survival from early lung cancer. Implications for screening Chest,” 101(4), pp. 1013–1018, 1992.
- [10] J. H. Austin, B. M. Romney, and L. S. Goldsmith, “Missed bronchogenic carcinoma: radiographic findings in 27 patients with a potentially resectable lesion evident in retrospect,” *Radiology*, 182(1), pp. 115–122, 1992.
- [11] P. K. Shah, J. H. Austin, C. S. White, P. Patel, L. B. Haramati, G. D. Pearson, M. C. Shiau, and Y. M. Berkmen, “Missed nonsmall cell lung cancer: radiographic findings of potentially resectable lesions evident only in retrospect,” *Radiology*, 226(1), pp. 235–241, 2003.
- [12] M. L. Giger, K. Doi, and H. MacMahon, “Image feature analysis and computer-aided diagnosis in digital radiography. 3. Automated detection of nodules in peripheral lung fields,” *Med. Phys.*, 15(2), pp. 158–166, 1988.
- [13] B. van Ginneken, B. M. ter Haar Romeny, and M. A. Viergever, “Computer-aided diagnosis in chest radiography: a survey,” *IEEE Trans. Med. Imag.*, 20(12), pp. 1228–1241, Dec. 2001.
- [14] K. Abe, K. Doi, H. MacMahon, M. L. Giger, H. Jia, X. Chen, A. Kano, and T. Yanagisawa, “Computer-aided diagnosis in chest radiography. Preliminary experience,” *Invest. Radiol.*, 28(11), pp. 987–993, 1993.
- [15] T. Kobayashi, X.W. Xu, H. MacMahon, C. E. Metz, and K. Doi, “Effect of a computer-aided diagnosis scheme on radiologists’ performance in detection of lung nodules on radiographs,” *Radiology*, 199(3), pp. 843–848, 1996.
- [16] S. Kakeda, J. Moriya, H. Sato, T. Aoki, H. Watanabe, H. Nakata, N. Oda, S. Katsuragawa, K. Yamamoto, and K. Doi, “Improved detection of lung nodules on chest radiographs using a commercial computer-aided diagnosis system,” *AJR Am J Roentgenol*, 182(2), pp. 505–510, 2004.

- [17] M. L. Giger, K. Doi, H. MacMahon, C. E. Metz, and F. F. Yin, "Pulmonary nodules: computer-aided detection in digital chest images," *Radiographics*, 10(1), pp. 41–51, 1990.
- [18] X. W. Xu, K. Doi, T. Kobayashi, H. MacMahon, and M. L. Giger, "Development of an improved CAD scheme for automated detection of lung nodules in digital chest images," *Med. Phys.*, 24(9), pp. 1395–1403, 1997.
- [19] W. A. Lampeter and J. C. Wandtke, "Computerized search of chest radiographs for nodules," *Invest. Radiol.*, 21(5), pp. 384–390, 1986.
- [20] S. C. Lo, S. L. Lou, J. S. Lin, M. T. Freedman, M. V. Chien, and S. K. Mun, "Artificial convolution neural network techniques and applications to lung nodule detection," *IEEE Trans. Med. Imag.*, 14(4), pp. 711–718, Dec. 1995.
- [21] J. S. Lin, S. C. Lo, A. Hasegawa, M. T. Freedman, and S. K. Mun, "Reduction of false positives in lung nodule detection using a two-level neural classification," *IEEE Trans. Med. Imag.*, 15(2), pp. 206–217, Apr. 1996.
- [22] C. E. Floyd, Jr., E. F. Patz Jr., J. Y. Lo, N. F. Vittitoe, and L. E. Stambaugh, "Diffuse nodular lung disease on chest radiographs: a pilot study of characterization by fractal dimension," *AJR. Am. J. Roentgenol.*, 167(5), pp. 1185–1187, 1996.
- [23] M. G. Penedo, M. J. Carreira, A. Mosquera, and D. Cabello, "Computer-aided diagnosis: a neural-network-based approach to lung nodule detection," *IEEE Trans. Med. Imag.*, 17(6), pp. 872–880, Dec. 1998.
- [24] F. Mao, W. Qian, J. Gaviria, and L. P. Clarke, "Fragmentary window filtering for multi scale lung nodule detection: preliminary study," *Acad. Radiol.*, 5(4), pp. 306–311, 1998.
- [25] M. Freedman, S. Lo, F. Lure, X. Xu, J. Lin, H. Zhao, T. Osicka, and R. Zhang, "Computer-aided detection of lung cancer on chest radiographs: algorithm performance vs. radiologists' performance by size of cancer," *Proc SPIE (Medical Imaging: Image Processing)*, pp. 150–159, 2001.
- [26] G. Coppini, S. Diciotti, M. Falchini, N. Villari, and G. Valli, "Neural networks for computer-aided diagnosis: detection of lung nodules in chest radiograms," *IEEE Trans. Inf. Technol. Biomed.*, 7(4), pp. 344–357, Dec. 2003.
- [27] B. Keserci and H. Yoshida, "Computerized detection of pulmonary nodules in chest radiographs based on morphological features and wavelet snake model," *Med. Image Anal.*, 6(4), pp. 431–447, 2002.
- [28] T. Matsumoto, H. Yoshimura, K. Doi, M. L. Giger, A. Kano, H. MacMahon, K. Abe, and S. M. Montner, "Image feature analysis of false-positive diagnoses produced by automated detection of lung nodules," *Invest. Radiol.*, 27(8), pp. 587–597, 1992.
- [29] D. L. Ergun, C. A. Mistretta, D. E. Brown, R. T. Bystriany, W. K. Sze, F. Kelcz, and D. P. Naidich, "Single-exposure dual-energy computed radiography: improved detection and processing," *Radiology*, 174(1), pp. 243–249, 1990.
- [30] F. Kelcz, F. E. Zink, W. W. Pepler, D. G. Kruger, D. L. Ergun, and C. A. Mistretta, "Conventional chest radiography vs dual-energy computed radiography in the detection and characterization of pulmonary nodules," *AJR. Am. J. Roentgenol.*, 62(2), pp. 271–278, 1994.
- [31] K. Suzuki, I. Horiba, and N. Sugie, "A simple neural network pruning algorithm with application to filter synthesis," *Neural Process. Lett.*, 13(1), pp. 43–53, 2001.
- [32] K. Suzuki, I. Horiba, N. Sugie, and M. Nanki, "Neural filter with selection of input features and its application to image quality improvement of medical image sequences," *IEICE Trans. Inf. Syst.*, vol. E85-D, (10), pp. 1710–1718, 2002.
- [33] K. Suzuki, S. G. Armato, F. Li, S. Sone, and K. Doi, "Massive training artificial neural network (MTANN) for reduction of false positives in computerized detection of lung nodules in low-dose CT," *Med. Phys.*, 30(7), pp. 1602–1617, 2003.
- [34] H. Arimura, S. Katsuragawa, K. Suzuki, F. Li, J. Shiraishi, S. Sone, and K. Doi, "Computerized scheme for automated detection of lung nodules in low-dose computed tomography images for lung cancer screening," *Acad. Radiol.*, 11(6), pp. 617–629, 2004.
- [35] K. Suzuki, J. Shiraishi, H. Abe, H. MacMahon, and K. Doi, "False-positive reduction in computer-aided diagnostic scheme for detecting nodules in chest radiographs by means of massive training artificial neural network," *Acad. Radiol.*, 12(2), pp. 191–201, 2005.
- [36] K. Suzuki, F. Li, S. Sone, and K. Doi, "Computer-aided diagnostic scheme for distinction between benign and malignant nodules in thoracic low-dose CT by use of massive training artificial neural network," *IEEE Trans. Med. Imag.*, 24(9), pp. 1138–1150, Sep. 2005.
- [37] K. Suzuki, I. Horiba, K. Ikegaya, and M. Nanki, "Recognition of coronary arterial stenosis using neural network on DSA system," *Syst. Comput. Japan*, 26(8), pp. 66–74, 1995.
- [38] D. E. Rumelhart, G. E. Hinton, and R. J. Williams, "Learning representations by back-propagating errors *Nature*," 323, pp. 533–536, 1986.
- [39] T. Ishigaki, S. Sakuma, Y. Horikawa, M. Ikeda, and H. Yamaguchi, "One-shot dual-energy subtraction imaging *Radiology*," 161(1), pp. 271–273, 1986.
- [40] G. M. Stephane, "A theory for multi scale approximation signal decomposition: the wavelet representation," *IEEE Trans. Pattern Anal. Mach. Intell.*, 11(7), pp. 674–693, Jul. 1989.
- [41] A. N. Akansu and R. A. Haddad, *Multi Scale Approximation Signal Decomposition*. Boston, MA: Academic, 1992.